

## FAR INFRARED IMAGING OF NGC 55

C. W. ENGELBRACHT<sup>1</sup>, K. D. GORDON<sup>1</sup>, G. J. BENDO<sup>1</sup>, P. G. PÉREZ-GONZÁLEZ<sup>1</sup>, K. A. MISSELT<sup>1</sup>, G. H. RIEKE<sup>1</sup>, E. T. YOUNG<sup>1</sup>, D. C. HINES<sup>1,3</sup>, D. M. KELLY<sup>1</sup>, J. A. STANSBERRY<sup>1</sup>, C. PAPOVICH<sup>1</sup>, J. E. MORRISON<sup>1</sup>, E. EGAMI<sup>1</sup>, K. Y. L. SU<sup>1</sup>, J. MUZEROLLE<sup>1</sup>, H. DOLE<sup>1</sup>, A. ALONSO-HERRERO<sup>1</sup>, J. L. HINZ<sup>1</sup>, P. S. SMITH<sup>1</sup>, W. B. LATTE<sup>2</sup>, A. NORIEGA-CRESPO<sup>2</sup>, D. L. PADGETT<sup>2</sup>, J. RHO<sup>2</sup>, D. T. FRAYER<sup>2</sup>, AND S. WACHTER<sup>2</sup>

*To appear in ApJS Spitzer Special Issue*

### ABSTRACT

We present images of the galaxy NGC 55 at 24, 70, and 160  $\mu\text{m}$  obtained with the Multiband Imaging Photometer for Spitzer (MIPS) instrument aboard the *Spitzer Space Telescope*. The new images display the far infrared emission in unprecedented detail and demonstrate that the infrared morphology differs dramatically from that at shorter wavelengths. The most luminous emission region in the galaxy is marginally resolved at 24 $\mu\text{m}$  and has a projected separation of nearly 520 pc from the peak emission in the optical and near infrared. This region is responsible for  $\sim 9\%$  of the total emission at 24  $\mu\text{m}$  and is likely a young star formation region. We show that this and other compact sources account for more than 1/3 of the total 24  $\mu\text{m}$  emission. We compute a total infrared luminosity for NGC 55 of  $1.2 \times 10^9 L_{\odot}$ . The star formation rate implied by our measurements is  $0.22 M_{\odot} \text{ yr}^{-1}$ . We demonstrate that the cold dust is more extended than the warm dust in NGC 55—the minor-axis scale heights are 0.32, 0.43, and 0.49 kpc at 24, 70 and 160  $\mu\text{m}$ , respectively. The dust temperature map shows a range of temperatures that are well-correlated with the 24  $\mu\text{m}$  surface brightness, from 20 K in low-surface-brightness regions to 26 K in high-surface-brightness regions.

*Subject headings:* galaxies: individual (NGC 55)—galaxies: ISM—infrared: galaxies

### 1. INTRODUCTION

NGC 55 is a dwarf ( $M_B = -18.6$ ) member of the Sculptor group, a nearby group dominated by spiral galaxies such as NGC 300 and the famous starburst NGC 253. At a distance of 1.78 Mpc (Karachentsev et al. 2003), the high inclination of NGC 55 ( $81^{\circ}$ ; Kiszkurko-Koziej 1988) makes it the nearest bright ( $m_B < 9$ ), edge-on galaxy. The galaxy is an analogue of the Large Magellanic Cloud, being of similar luminosity, morphological type (SB(s)m), and metallicity ( $12 + \log(O/H) = 8.33$ ; Schmidt & Boller 1993).

The energetic star formation, proximity, and high surface brightness of NGC 55 have made it a popular target for ISM studies, both of the neutral (e.g., Puche, Carignan, & Wainscoat 1991) and ionized component (e.g., Hoopes, Waltherbos, & Greenawalt 1996; Ferguson, Wyse, & Gallagher 1996). The galaxy is known to host extraordinary H II regions both in (Tüllmann & Rosa 2004) and out of the disk (Tüllmann et al. 2003).

NGC 55 was observed as part of the Multiband Imaging Photometer for Spitzer (MIPS) instrument commissioning activities (Rieke et al. 2004). NGC 55 has a large ( $\sim 30'$ ) but well-defined angular extent and so was chosen to test the imaging capabilities of the instrument on extended sources with both high and low surface brightness regions. These commissioning observations proved to be of sufficient quality to support scientific analysis. In this paper, we measure global properties of the galaxy (temperature, luminosity, scale height as a function of wavelength, and star formation rate) and exploit the sen-

sitivity and resolution of MIPS to determine the distribution of temperatures and luminosities within the galaxy and to address the nature of the nuclear source. We refer to other papers in this volume for topics best studied in more face-on galaxies: 1.) Star formation rate indicators in M 81 (Gordon et al. 2004b); 2.) Location of stochastically heated PAH dust grains in NGC 300 (Helou et al. 2004); 3.) Heating of cold dust in M 33 (Hinz et al. 2004).

### 2. OBSERVATIONS AND DATA REDUCTION

Images of NGC 55 at 24, 70, and 160  $\mu\text{m}$  were obtained with MIPS on 2003 November 30 (PROGID = 718, AORKEY = 8085504, 8100352). 3232 individual images at each of the three MIPS bands were taken, with an exposure time of approximately 4 seconds per image. The depth of the map at each point was 240, 120, and 24 seconds at 24, 70, and 160  $\mu\text{m}$ , respectively. The resulting mosaics cover an area of approximately  $30' \times 60'$  at each wavelength, with a region in common to all three wavelengths of  $30' \times 30'$ .

The MIPS images were reduced using the MIPS Instrument Team Data Analysis Tool which is the test bed for data reduction algorithms for MIPS (Gordon et al. 2004a). The data were reduced as described in that paper, with some minor exceptions: a customized flat field was required at 24  $\mu\text{m}$ , and a time-dependent illumination correction and calibration lamp latent image removal were required at 70  $\mu\text{m}$ . The uncertainties on the calibration are estimated at 10%, 20%, and 20% for 24, 70, and 160  $\mu\text{m}$ , respectively (cf. Rieke et al. 2004). These uncertainties are dominated by the uncertainty in the absolute calibration—uncertainties in the background level for this target are around 5% and so have not been included in subsequent analysis. The final MIPS mosaics are displayed in Fig. 1.

<sup>1</sup> Steward Observatory, University of Arizona, Tucson, AZ 85721

<sup>2</sup> Spitzer Science Center, California Institute of Technology, Pasadena, CA 91125

<sup>3</sup> Space Science Institute, 4750 Walnut Street, Suite 205, Boulder, CO 80301

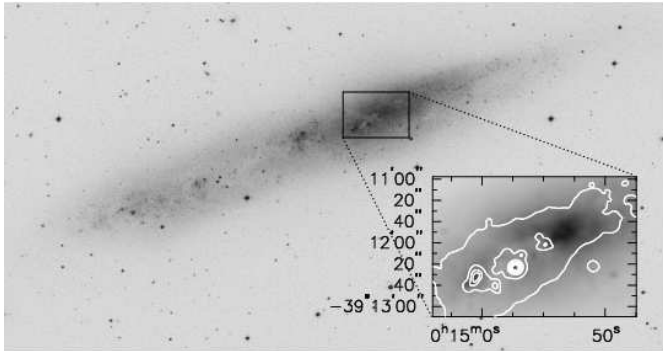


FIG. 2.— Digitized Sky Survey image of NGC 55. The inset shows the I band image (obtained from the NASA/IPAC Extragalactic Database and attributed there to B. Madore) in a linear stretch. Plotted over the I band image are  $24\ \mu\text{m}$  contours in evenly-spaced intervals from 50 to  $4000\ \mu\text{Jy arcsec}^{-2}$ . The I band image has been convolved to match the  $24\ \mu\text{m}$  resolution.

The beam sizes in the three MIPS bands are limited by diffraction and so vary with wavelength: The FWHM of the point-spread-function (PSF) is 6, 18, and  $40''$  at 24, 70, and  $160\ \mu\text{m}$ , respectively. Where images have been compared directly at different wavelengths, they have been convolved to matching resolutions (the  $160\ \mu\text{m}$  resolution, unless otherwise noted) using kernels derived from PSF models generated using the TinyTim software (Krist 2002).

### 3. RESULTS

#### 3.1. Morphology

The morphology of the galaxy in the MIPS images is broadly similar, being dominated by a bright central region and asymmetric emission from the disk on either side. The extent of the galaxy (both in the optical and far infrared (FIR)) is  $\sim 9'$  to the NW of the nuclear region and  $\sim 15'$  to the SE. The central region and the region to the SE are separated by a low-surface-brightness gap that crosses the galaxy at  $\alpha(2000) \sim 00^{\text{h}}15^{\text{m}}08^{\text{s}}$ . The  $24\ \mu\text{m}$  emission is dominated by discrete regions, in contrast to the smoother structure seen at 70 and  $160\ \mu\text{m}$ . These discrete emission regions also dominate the nuclear region (which we have assumed lies at the  $24\ \mu\text{m}$  peak), as demonstrated by Figure 2.

#### 3.2. Discrete Sources

We performed photometry on the  $24\ \mu\text{m}$  image using the DAOPhot package in IRAF<sup>4</sup>. The luminosities of the extracted point sources are plotted in Figure 3, where we simply multiplied the measured flux density by the  $24\ \mu\text{m}$  bandpass to determine the in-band flux and thence the luminosity. We have made a correction for the background point sources in the NGC 55 image by subtracting the luminosity function measured in a background region of identical size, well away from the galaxy. The integrated flux of the extracted point sources is more than 1/3 of the total  $24\ \mu\text{m}$  emission from this galaxy.

The brightest point source is located near the center of NGC 55. As demonstrated by Figure 2, this  $24\ \mu\text{m}$  peak

<sup>4</sup> IRAF is distributed by the National Optical Astronomy Observatories, which are operated by the Association of Universities for Research in Astronomy, Inc., under cooperative agreement with the National Science Foundation.

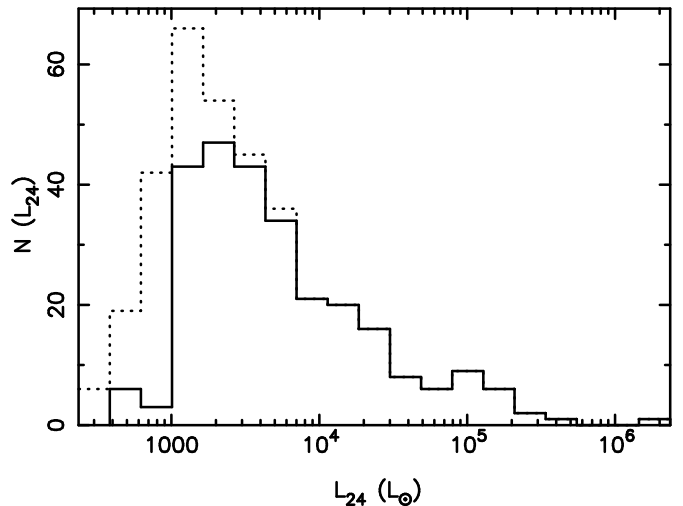


FIG. 3.— Luminosity distribution of discrete  $24\ \mu\text{m}$  emission regions. The dotted line represents the raw histogram while the solid line represents the luminosity function after correction for background sources.

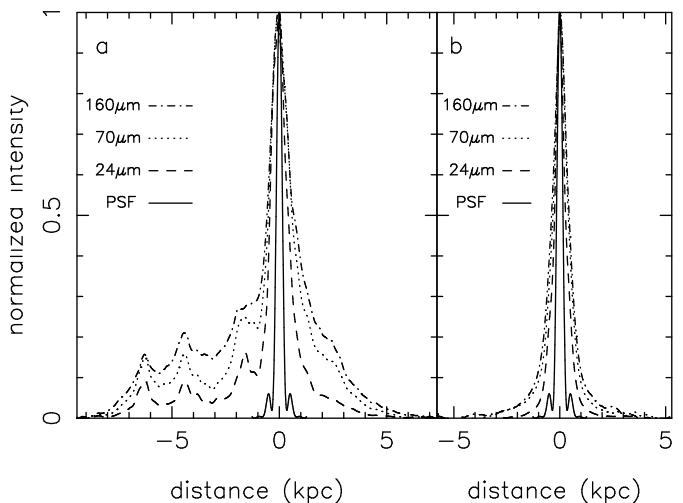


FIG. 4.— Surface brightness profiles along the major (a) and minor (b) axes of NGC 55, plotted on a linear scale. The major-axis profile runs E to W along the disk while the minor-axis profile runs S to N across the disk.

is nearly an arcminute (a projected separation of 520 pc) away from the peak I-band emission. This source appears to be hidden behind a strong dust lane apparent in the I-band image and is responsible for  $\sim 9\%$  of the total emission at  $24\ \mu\text{m}$ . This source is marginally resolved at  $24\ \mu\text{m}$ —the measured FWHM of the source is  $\sim 5''.3$ .

#### 3.3. Major and Minor Axis Profiles

The edge-on aspect of the galaxy provides a unique opportunity to measure infrared scale heights. We generated profiles along the major and minor axes of NGC 55 by averaging the images (convolved to the  $160\ \mu\text{m}$  resolution) parallel and perpendicular to the disk of the galaxy. These profiles are presented in Figure 4, in which the PSF measured on an unresolved galaxy in the field is plotted for reference. The profiles have all been normalized to the same peak value.

The extent of the observed emission is correlated with

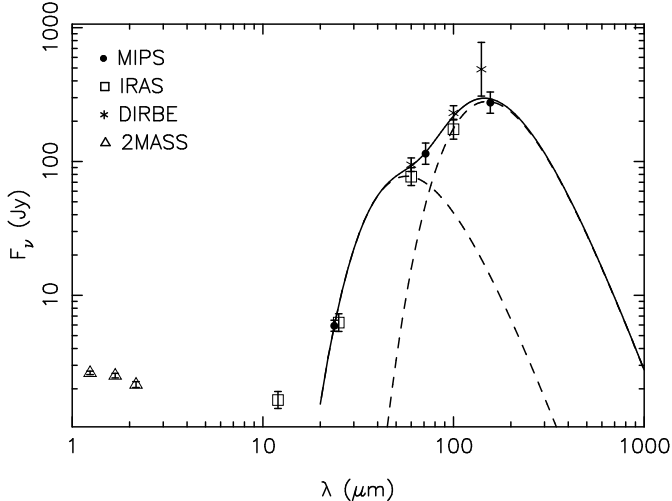


FIG. 5.— Infrared SED of NGC 55. The dashed lines are modified blackbody curves (emissivity  $\sim \lambda^{-2}$ ) at 51 K and 19 K, while the solid line is the sum of the two dashed curves.

wavelength: the emission is more extended at longer wavelengths, along both the major and minor axes. The major-axis profile is highly asymmetric, with an off-center nuclear region and discrete emission regions evident in the eastern portion of the disk. The minor-axis profile is more symmetric, and we fit it with a function proportional to  $\exp(-x/h)$ , where  $x$  is the distance from the emission peak and  $h$  is the scale height. The scale height is 0.32, 0.43, and 0.49 kpc at 24, 70 and 160  $\mu\text{m}$ . These values are higher than the value of 0.10 – 0.21 kpc determined by Kizskurno-Koziej (1988) for the stellar component of NGC 55 but are comparable to the 0.37 – 0.45 kpc scale height for the ionized gas determined by Miller & Veilleux (2003).

### 3.4. Spectral Energy Distribution

We computed the FIR SED of NGC 55 using MIPS data, combined with measurements by the Infrared Astronomical Satellite (IRAS), the Diffuse Infrared Background Experiment (DIRBE), and the Two Micron All Sky Survey (2MASS). The total emission in the MIPS images was measured using IRAF’s “polyphot” task, while the IRAS measurements were taken from Rice et al. (1988). The DIRBE measurements were computed using the DIRBE Point Source Photometry Research Tool<sup>5</sup>, and the 2MASS measurements were taken from Jarrett et al. (2003). We fit the fluxes with two modified blackbody functions to characterize roughly the dust temperature and found a good fit with two components at 51 K and 19 K, modified by a  $\lambda^{-2}$  emissivity (adopted as an appropriate factor beyond 70  $\mu\text{m}$ ; cf. Draine 2003). The data and the fit are plotted in Figure 5.

The total infrared (TIR) luminosity was estimated from both the MIPS and IRAS fluxes using equations 4 and 5 of Dale & Helou (2002), respectively; both equations indicate the luminosity of NGC 55 is  $1.14 \times 10^9 L_{\odot}$ . Additionally, the bolometric IR luminosity was computed from the data directly, integrating the two-

temperature blackbody fit discussed above (plus a linear fit to the 2MASS and 12  $\mu\text{m}$  data where the blackbody falls short of the observed emission) from 3–1100  $\mu\text{m}$  to compute a luminosity of  $1.29 \times 10^9 L_{\odot}$ . We have averaged these three estimates to compute  $L_{TIR} = 1.2 \times 10^9 L_{\odot}$ . The star formation rate implied by this luminosity is  $0.22 M_{\odot} \text{ yr}^{-1}$ , using equation 4 of Kennicutt (1998). This rate is roughly 40% higher than the value derived from H $\alpha$  measurements (Ferguson, Wyse, & Gallagher 1996).

We compute a total infrared luminosity of  $1.2 \times 10^8 L_{\odot}$  for the brightest compact source discussed in § 3.2 using the formula discussed above after making an aperture correction of 2.5 (computed using the PSF model discussed in § 2). This value depends on a large aperture correction, so we have compared it to the value obtained by assuming that the SED of the integrated galaxy is similar to that of the compact source (measured at the native 24  $\mu\text{m}$  resolution) and that we can therefore scale the 24  $\mu\text{m}$  emission to a TIR luminosity. Since this source contributes  $\sim 9\%$  of the flux at 24  $\mu\text{m}$ , the integrated luminosity implied by taking this same fraction of  $L_{TIR}$  is  $1.1 \times 10^8 L_{\odot}$ , similar to the value derived above. This large luminosity is similar in scale to the nuclear star formation regions in M 33 and the Galactic Center discussed by Gordon et al. (1999), and we suggest that the nuclear source in NGC 55 is similarly powered by star formation. The high infrared and H $\alpha$  luminosity ( $9 \times 10^{39} \text{ erg s}^{-1}$  (Ferguson, Wyse, & Gallagher 1996)) of the central source can be plausibly attributed to star formation if we are observing a very young burst: the output is similar to a Starburst99 (Leitherer et al. 1999) model ( $M = 10^5 M_{\odot}$ ,  $\alpha = 2.35$ ,  $Z = 0.004$ ) at an age of 2 Myr. The star formation scenario for the central source is also consistent with mid-infrared spectroscopic (Thornley et al. 2000), radio (Hummel et al. 1986), and x-ray (Ranalli et al. 2003) observations of this galaxy.

### 3.5. Dust Content

We have used the 70 and 160  $\mu\text{m}$  images to characterize the dust temperature in NGC 55. We fit a blackbody modified by a  $\lambda^{-2}$  emissivity function to each pixel and assigned a temperature to that pixel based on the temperature of the best fit. In reality, multiple dust temperature components are expected to contribute to the far-infrared emission (Dale & Helou 2002), but this approach allows us to characterize variations across the disk of the galaxy. The result is shown in Figure 6. The mean temperature of this map (22.6 K) is similar to the value of 22 K computed by Bendo et al. (2003) from the central area covered by the single ISO 60 and 100  $\mu\text{m}$  pointing.

The temperatures range from 20 to 26 K and correlate well with the FIR surface brightness, with the exception of a few streaks in the temperature map which correspond to artifacts in the 70 and 160  $\mu\text{m}$  images. The highest dust temperatures in Figure 6 correspond to peaks in the 24  $\mu\text{m}$  emission and are likely H II regions (cf. Hinz et al. 2004; Gordon et al. 2004b) while the lowest temperatures correspond to diffuse regions with little star formation.

## 4. CONCLUSION

We have presented observations of the galaxy NGC 55 at 24, 70, and 160  $\mu\text{m}$  made with the MIPS instru-

<sup>5</sup> <http://lambda.gsfc.nasa.gov/product/cobe/browser.cfm>

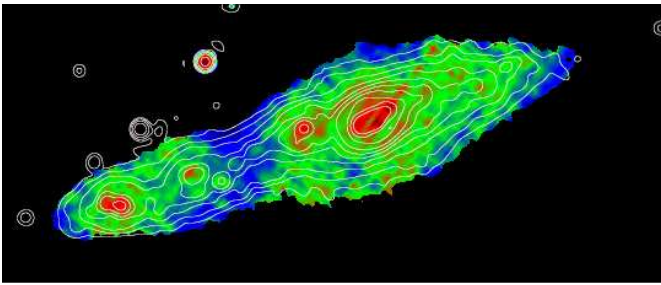


FIG. 6.— Temperature map of NGC 55. The color stretch ranges from 19 K (blue) to 27 K (red), and the image has been clipped to exclude regions of low signal-to-noise ratio in the 70 and 160  $\mu\text{m}$  bands. The contours show the 24  $\mu\text{m}$  emission, convolved to the 160  $\mu\text{m}$  resolution as described in the text, in 10 logarithmically-spaced levels from 1.5 to 200  $\mu\text{Jy arcsec.}^{-2}$ .

ment aboard the *Spitzer Space Telescope*. The data provide images at unprecedented sensitivity and resolution at these wavelengths. The data demonstrate that the brightest region at FIR wavelengths is faint at optical wavelengths and has a projected separation from the optical peak of nearly 520 pc. The FIR peak is barely resolved in the 6'' 24  $\mu\text{m}$  beam but still accounts for  $\sim 9\%$  of the total flux at that wavelength. Comparison of the infrared luminosity of this source and H $\alpha$  measurements from the literature to a starburst model suggest that the current episode of star formation could be as young as 2 Myr.

The TIR luminosity of the galaxy measured in several ways is  $1.2 \times 10^9 L_{\odot}$ , implying a star formation rate of

$0.22 M_{\odot} \text{ yr}^{-1}$ . 10% of the infrared luminosity is due to the compact nuclear source, which is of comparable luminosity to the bright star formation regions at the center of M 33 and the Milky Way. The integrated flux of this source and the other compact sources in the galaxy accounts for more than 1/3 of the 24  $\mu\text{m}$  emission from NGC 55. A dust temperature map shows that the temperature ranges from 20 K in the low-surface-brightness region SE of the nucleus to 26 K in the nucleus and other star-formation regions in the disk.

The authors wish to thank M. Blaylock and J. Cadien for their expert assistance with processing the MIPS data presented here.

This work is based in part on observations made with the Spitzer Space Telescope, which is operated by the Jet Propulsion Laboratory, California Institute of Technology under NASA contract 1407. Support for this work was provided by NASA through Contract Number 960785 issued by JPL/Caltech.

This research has made use of the the NASA/IPAC Extragalactic Database (NED) and the NASA/IPAC Infrared Science Archive, which are operated by the Jet Propulsion Laboratory, California Institute of Technology, under contract with the National Aeronautics and Space Administration.

This research used the DIRBE Point Source Photometry Research Tool, a service provided by the Legacy Archive for Microwave Background Data at NASA's Goddard Space Flight Center.

#### REFERENCES

- Bendo, G. J., Joseph, R. D., Wells, M., Gallais, P., Haas, M., Heras, A. M., Klaas, U., Laureijs, R. J., Leech, K., Lemke, D., Metcalfe, L., Rowan-Robinson, M., Schulz, B., Telesco, C. 2003, *AJ*, 125, 2361
- Dale, D. A. & Helou, G. 2002, *ApJ*, 576, 159
- Draine, B. T. 2003, *ARA&A*, 41, 241
- Ferguson, A. M. N., Wyse, R. F. G., & Gallagher, J. S. 1996, *AJ*, 112, 2567
- Gordon, K. D., Hanson, M. M., Clayton, G. C., Rieke, G. H., & Misselt, K. A. 1999, *ApJ*, 519, 165
- Gordon, K. D. 2004, *PASP*, submitted
- Gordon, K. D. 2004, *ApJS*, this volume
- Helou, G. 2004, *ApJS*, this volume
- Hinz, J. L. 2004, *ApJS*, this volume
- Hoopes, C. G., Walterbos, R. A. M., & Greenawalt, B. E. 1996, *AJ*, 112, 1429
- Hummel, E., Dettmar, R.-J., & Wielebinski, R. 1986, *A&A*, 166, 97
- Jarrett, T. H., Chester, T., Cutri, R., Schneider, S. E., & Huchra, J. P. 2003, *AJ*, 125, 525
- Karachentsev, I. D., Grebel, E. K., Sharina, M. E., Dolphin, A. E., Geisler, D., Guhathakurta, P., Hodge, P. W., Karachentseva, V. E., Sarajedini, A. & Seitzer, P. 2003, *A&A*, 404, 93
- Kennicutt, R. C., Jr. 1998, *ARA&A*, 36, 189
- Kizskurno-Koziej, E. 1988, *A&A*, 196, 26
- Krist, J. 2002, "TinyTIM/SIRTF User's Guide", Spitzer Science Center internal document
- Leitherer, C., et al. 1999, *ApJS*, 123, 3
- Miller, S. T. & Veilleux, S. 2003, *ApJ*, 148, 383
- Puche, D. & Carignan, C. 1988, *AJ*, 95, 1025
- Puche, D., Carignan, C., & Wainscoat, R. J. 1991, *AJ*, 101, 447
- Ranalli, P., Comastri, A., & Setti, G. 2003, *A&A*, 399, 39
- Rice, W., Lonsdale, C. J., Soifer, B. T., Neugebauer, G., Koplan, E. L., Lloyd, L. A., de Jong, T., & Habing, H. J. 1988, *ApJS*, 68, 91
- Rieke, G. H., et al. 2004, *ApJS*, this volume
- Schmidt, K.-H. & Boller, T. 1993, *AN*, 314, 361
- Thornley, M. D., Förster Schreiber, N. M., Lutz, D., Genzel, R., Spoon, H. W. W., Kunze, D., & Sternberg, A. 2000, *AJ*, 539, 641
- Tüllmann, R., Rosa, M. R., Elwert, T., Bomans, D. J., Ferguson, A. M. N., & Dettmar, R.-J. 2003, *A&A*, 412, 69
- Tüllmann, R. & Rosa, M. R. 2004, *A&A*, 416, 243

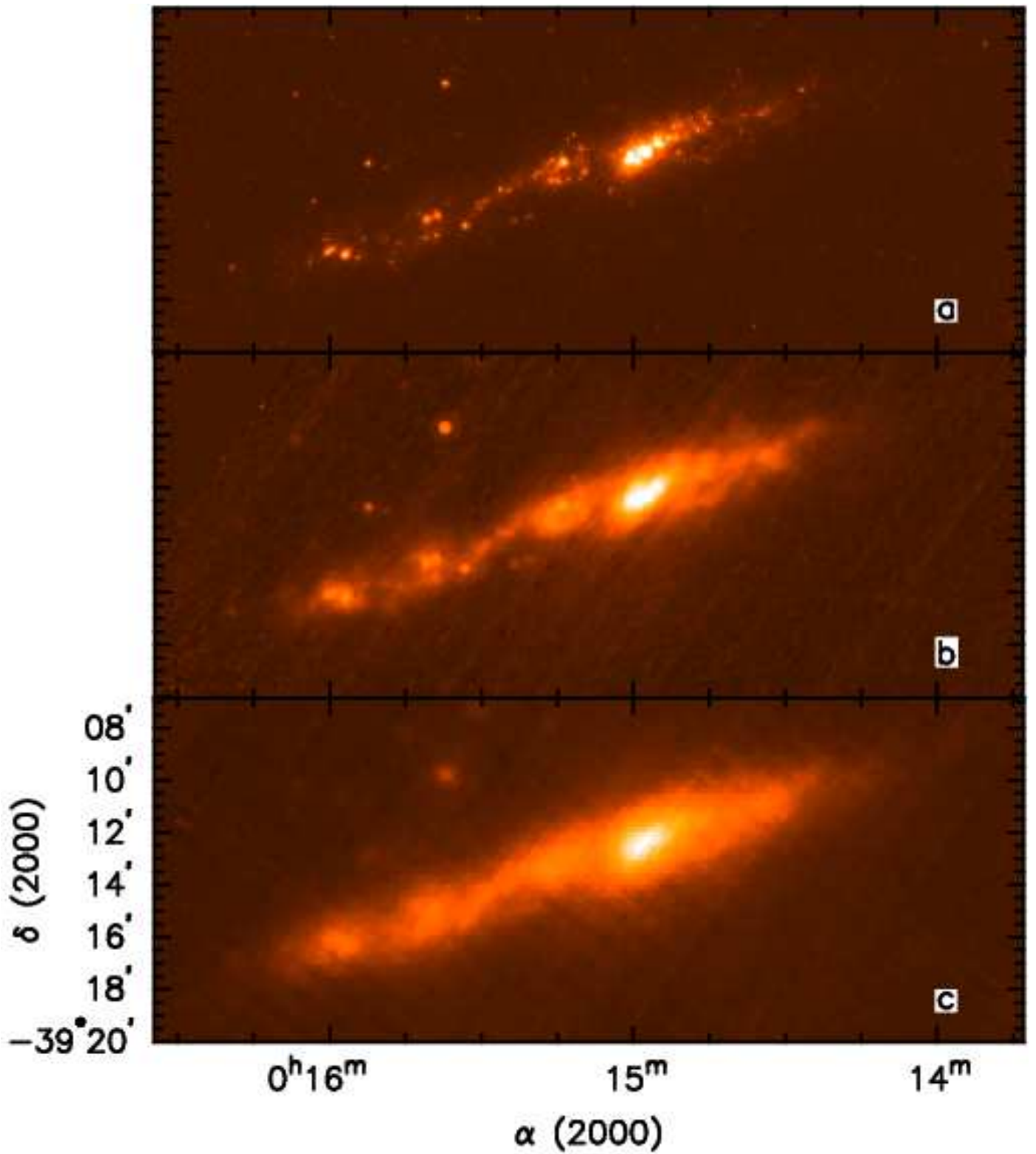


FIG. 1.— Images of NGC 55 at  $24 \mu\text{m}$  (a),  $70 \mu\text{m}$  (b), and  $160 \mu\text{m}$  (c), presented in an asinh stretch to compress the dynamic range.